affected by the seeding. The clouds in this area were glaciated, nearly featureless, and consisted almost entirely of unrimed and unaggregated ice particles (thick plates, columns, bullets, and irregular crystals) present in high concentrations. While flying over this area, we observed the unusual paranthelic circle (that is, a white horizontal arc passing through both the antisolar and subsolar points) (see cover, bottom right); this is caused by external reflections in uniformly sized ice crystals. The oblique arcs crossing the paranthelic circle at the antisolar points do not appear to have been previously reported. In clouds sampled just south of the seeded area, supercooled water droplets coexisted with ice particles.

Calculations based on the rawinsonde measurements, the dispersal of the silver iodide, and the trajectories of the solid precipitation particles indicated that the artificial seeding was unlikely to have affected the precipitation reaching Alpental. However, at Hyak and Keechelus Dam there was an excellent chance that most of the crystals reaching the ground would have been affected by the seeding between about 1310 to 1450 and 1315 to 1510 hours, respectively.

The crystal types reaching Alpental did not change significantly throughout the day, but their degree of riming increased from 1300 to 1530 hours (Fig. 2a). Moreover, the precipitation rate was fairly steady at about 0.025 cm of water per hour until 1500 hours when a sharp increase to 0.089 cm per hour occurred. At Hyak, on the other hand, riming was completely absent during and after the PPE of the seeding at this station (Figs. 1d and 2b). Perhaps even more significant, several new crystal types (sectors, plates, and "germs"), which grow at the relatively low supersaturations to be expected in the seeded clouds, fell at Hyak during the PPE and disappeared after the PPE. It was precipitating steadily at Hyak prior to 1300 hours but near the start of the PPE precipitation virtually ceased; at 1400 hours very light precipitation started again. At Keechelus Dam (Fig. 2c) new crystal types (plates, bullets, side planes, and broad-branched crystals) appropriate to low supersaturations also appeared during the PPE and disappeared afterward. Precipitation at Keechelus Dam was light and sporadic throughout the day. Precipitation rates obtained from a recording gauge at Kachess Dam showed that the only precipitation of the day at this station fell during the PPE (Fig. 2d); the rates correspond to moderate drizzle. Measurements between 1100 and 1600 hours of the concentrations of freezing nuclei in the snow which fell at Hyak and Keechelus Dam showed a maximum concentration at 1330 hours at Hyak, and at Keechelus Dam increases in the concentrations of ice nuclei occurred after 1315 hours.

In summary, we have documented a chain of physical events both in the clouds and on the ground which confirm the predicted effects of the artificial seeding. Cloud particles collected from the aircraft and observed optical effects showed conclusively that the seeding promoted glaciation in the clouds upwind and over the target area. Trajectory analysis showed that the effects of seeding should have been observed on the ground at Hyak, Keechelus Dam, and Kachess Dam. At Hyak, riming ceased completely, new crystals appeared, and the precipitation rate decreased dramatically during the PPE. We conclude that this was due to the fact that the bulk of the unrimed ice crystals produced by seeding were carried over the Cascade crest. At Keechelus Dam, situated to the east of the crest, new crystal types which could be traced back to the seeded clouds, appeared during the PPE. At Kachess Dam, situated about 20 km downwind of the crest, the only snowfall of the day fell during the PPE, and we attribute this to the effects of seeding diverting the snowfall across the Cascade crest.

We have obtained results similar to those described above on other occasions during extensive studies over the past 3 years. However, although in most cases seeding has produced observable modifications to the clouds, we have often failed to observe appreciable changes in precipitation within our small target area on the ground. We conclude, therefore, that, although prospects for modifying and redistributing precipitation by cloud seeding across mountain ranges similar to those of the Cascades appear reasonably good, this technique has not yet reached the point where it can be used as a reliable method for the controlled redistribution of precipitation within a small predetermined target area.

PETER V. HOBBS
L. F. RADKE
Atmospheric Sciences Department, University of Washington, Seattle 98195

References and Notes

1. P. V. Hobbs, R. C. Easter, A. B. Fraser, *J. Atmos. Sci.*, in press.
2. P. V. Hobbs, L. F. Radke, J. Locatelli, C. Robertson, R. Farber, D. A. Burrows, *Contrib. Cloud Phys. Group Univ. Wash. Res. Rep. 5* (1970).
3. P. V. Hobbs, L. F. Radke, R. R. Brown, in preparation.
4. Ice particles are categorized according to the scheme suggested by C. Magono and C. W. Lee, *J. Fac. Sci. Hokkaido Univ. Ser. 7* **2**, 321 (1966).
5. We thank all the members of the Cloud Physics Group at the University of Washington for their valuable help. This work was supported by the Division of Atmospheric Water Resources Management, Department of the Interior, under contract No. 14-06-D-6999 and by the RANN Program of the National Science Foundation (grant GA-27637). Contribution No. 286, Atmospheric Sciences Department, University of Washington.

9 February 1973; revised 28 March 1973

Climatic Change on Mars

Abstract. *The equatorial sinuous channels on Mars detected by Mariner 9 point to a past epoch of higher pressures and abundant liquid water. Advective instability of the martian atmosphere permits two stable climates—one close to present conditions, the other at a pressure of the order of 1 bar depending on the quantity of buried volatiles. Variations in the obliquity of Mars, the luminosity of the sun, and the albedo of the polar caps each appear capable of driving the instability between a current ice age and more clement conditions. Obliquity driving alone implies that epochs of much higher and of much lower pressure must have characterized martian history. Climatic change on Mars may have important meteorological, geological, and biological implications.*

Mars is the only known planet with a major atmospheric constituent condensable at typical surface temperatures; they range from 290°K at equatorial noon to a temperature at the cold pole, $T_p \simeq 145$°K in polar winter—a temperature below the frost point of CO_2, which constitutes over 90 percent of the atmosphere. In a pre–Mariner 9 discussion, one of us (*1*) proposed that Mars is currently in an ice age, that more clement conditions prevailed earlier, and that Mars oscillates between these two climatic states. A time of higher pressures, P, higher temperatures, and

larger quantities of liquid water was envisioned, with the earlier atmosphere now frozen out in the polar caps.

The frequency-diameter curve for impact craters on Mars, obtained from Mariner 9 imagery, exhibits two marked changes in slope between 5 and 20 km for heavily cratered regions; the statistics imply a period of early intense erosion, a long intermediate epoch of lesser erosion, and relatively little erosion and deposition within craters over the last $\sim 10^9$ years (*2*). While there is little aqueous transport on Mars today, eolian transport and abrasion are very efficient (*3*). Earlier epochs of more intense erosion would appear to require other efficient erosion mechanisms. The only such mechanism known on the earth is aqueous. The sharpness of the slope change suggests that earlier erosion mechanisms were turned off in much less than 10^9 years. The apparent widespread hydration of martian surface minerals (*4*) has been confirmed from aircraft infrared spectroscopy (*5*), evoking an earlier suggestion that such water of crystallization may be indicative of a past warmer and wetter Mars (*6*). An analysis (*7*) of the Mariner 9 infrared spectrometer (IRIS) data weakly suggests abundant clays on Mars and a similar past.

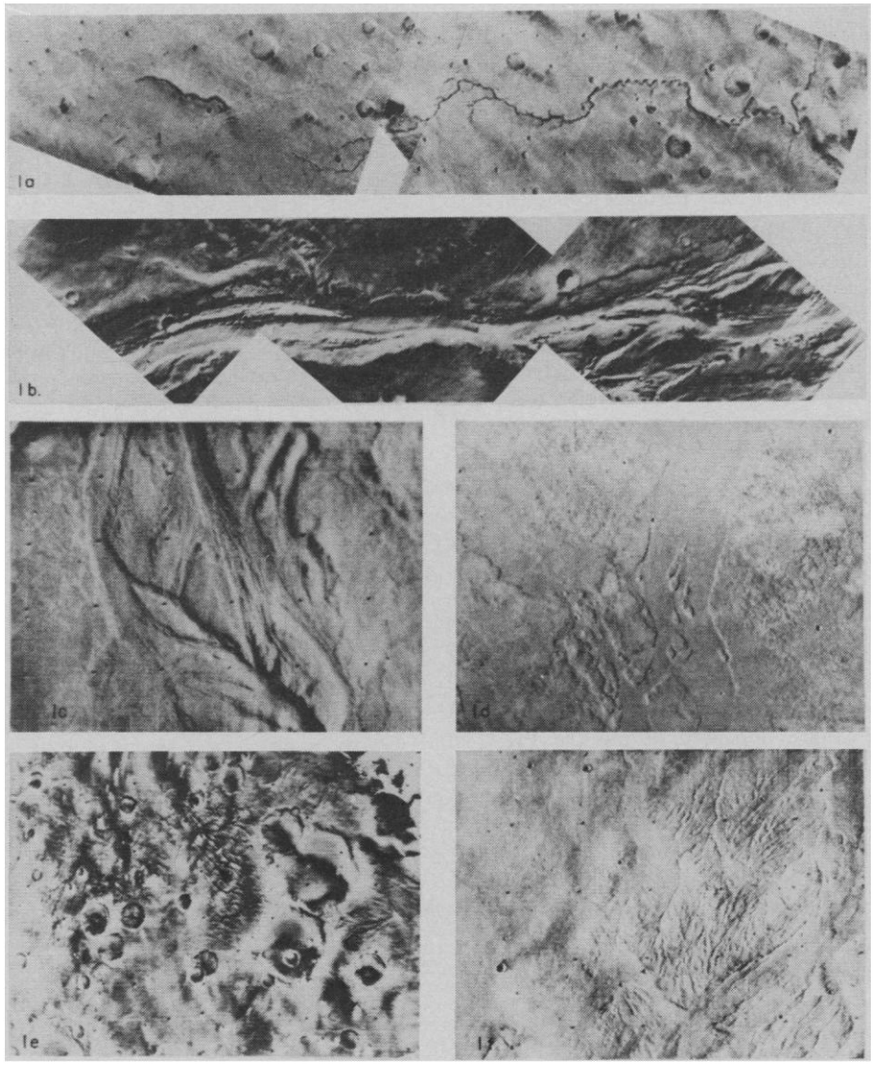

Fig. 1. Mariner 9 photographs indicative of running water on Mars. The details of flow—for example, whether produced by rainfall or underground rivers—differ from case to case. (a) Mosaic of sinuous dendritic channel system in Mare Erythraeum (29°S, 40°W), $\sim$ 1000 km long. Note the evidence of tributaries buried under sand and the possible covered segment of the main channel at left [Image Processing Laboratory product, pictures 122/6354843, 131/6283023, 211/9160800]. (b) Mosaic of about one-third ($\sim$ 120 km) of the Amazonis-Memnonia channel. This segment, exhibiting banks, bars and braids, is centered at 7°S, 151°W [Mission Test Video System product, revolution 458, pictures 12499650, 12499720, 12499790]. (c) Narrow-angle (B-frame) close-up of braided portion of Amazonis-Memnonia channel at 6°S, 150°W. The feature, about 40 km across, is reminiscent of the results of episodic flooding in terrestrial river systems [MTVS product, picture 224/9628649]. (d) Teardrop-shaped islands $\sim$ 5 km long in a channel between Aetheria and Elysium (31°N, 229°W) [IPL product, picture 204/8910729]. Similar streamlined islands in the Lunae Palus channel darkened during the Mariner 9 mission, probably due to deflation of bright overlying dust by winds coursing down the channel (*3*). (e) Network of gullies in Sabaeus Sinus (10°S, 330°W) on old cratered terrain, suggestive of cutting by rainfall. The field of view is $\sim$ 600 km across [MTVS product, picture 423/11620533]. (f) Possible mountain drainage system in Alba (45°N, 116°W). This is not a perfect replica of terrestrial mountain drainage systems because some of the flow appears to be uphill, which poses interpretation problems with all hypothesized liquids. The field of view is $\sim$ 70 km across [MTVS product, picture 152/7039903].

By far the most striking evidence for earlier more clement conditions on Mars is the discovery by Mariner 9 imagery of many cut channels on the planet. These channels exhibit sinuosities, dendritic patterns corresponding in some cases to third- and fourth-order tributary systems, streamlined "islands" within the channels, and an intricate braided structure reminiscent of terrestrial river basins characterized by intermittent flow (Fig. 1). These features and the lack of correlation of the termini of channels with craters are uncharacteristic of high-viscosity excavation of channels, as in collapsed lava tubes on the earth and perhaps on the moon. Some features like terrestrial lava tubes are found on Mars, but are not discussed further here. While the largest martian channels are hundreds of kilometers long, there are also intricate networks of very fine channels on the slopes of old cratered terrains (Fig. 1). From IRIS elevation data (*8*) the largest martian channel, that in Memnonia-Amazonis, flowed downhill toward the equator. At least two of the channels in Chryse appear to be connected with chaotic terrain—probably thermokarst produced by melting of underlying permafrost, subsurface water transport, and the subsequent collapse of the overburden (*9*). Such features may be produced by underground rivers, but many other channels can only be understood by surface flow. Rainfall is not required in this discussion. Flow for many hundreds to more than a thousand kilometers cannot occur at a pressure of 6 mbar because the evaporation rate prevents large transport distances. But the source of the water can either be above or below, and some of the water sources may very well be subsurface geothermal penetrations of permafrost.

The distribution of such channels

visible over the surface of Mars at a limiting resolution of $\geqq 1$ km is displayed in Fig. 2. There is a striking peak a few degrees north of the equator. The decline in the abundance of channels toward high latitudes must be due to either their infrequent formation or their efficient removal. While there is evidence of an increase in the mantling of the surface by fine debris with increasing latitude (*10*), the effect is too gentle to explain (Fig. 2). The only plausible material of low viscosity and high cosmic abundance which could excavate channels and which has a phase diagram in which martian equatorial temperatures are important is liquid water (*11*). Even today, daytime equatorial temperatures are above the freezing point of water. The distribution function in Fig. 2 may reflect preferential equatorial rainfall on earlier Mars as on contemporary earth, and the concentration of tectonic features toward the north equatorial zone. From the cratering statistics in the channel areas, at least many channels are $\geqq 3 \times 10^8$ years old.

Several lines of evidence thus point to a past more clement epoch on Mars. We here present a specific model capable of giving reversible major climatic fluctuations and P well above the triple point pressure of water, 6.11 mbar. The general circulation of the present martian atmosphere carries heat poleward, but the quantity of heat carried and the efficiency of heat exchange between the atmosphere and the ground are both so small that the effect is to heat the polar cap by a few degrees Kelvin at most. On the other hand the present P is quite close to the vapor pressure above the cold pole of the planet (*12*), and it seems likely that this mechanism—analogous to a cold finger in a laboratory gas handling system—determines the total pressure on the planet. We employ a model of advective meridional eddy heat flux, in winter by baroclinic waves, which reproduces well the results of numerical circulation models; we describe this model in more detail elsewhere (*13*). A small increase in the heat absorbed by the polar cap increases P and thereby improves the efficiency of atmospheric heat transport. This in turn heats the pole further, and increases P once again. The critical parameter is the flux of solar energy absorbed at the pole

$$S = S_0 a^{-2}(1 - e^2)^{-1/2}(\sin\delta/\pi)(1 - A) \quad (1)$$

where S_0 is the solar constant at 1 A.U., a is the semimajor axis of the martian orbit in astronomical units, e is the orbital eccentricity, δ is the obliquity of Mars, and A is the frequency-integrated albedo of the polar cap.

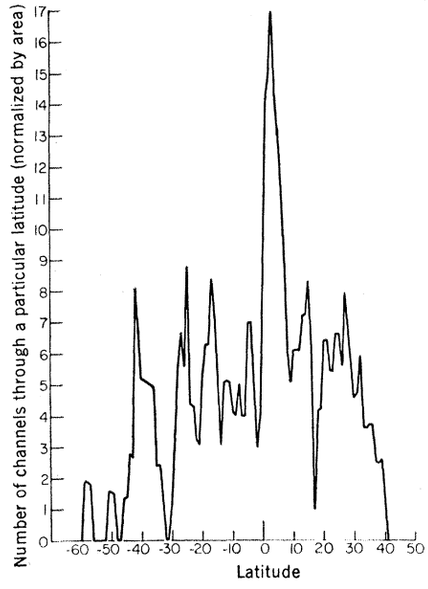

Fig. 2. A distribution function of Mariner 9 channels, visible at wide-angle (A-frame) resolution, as a function of latitude. The distribution has been properly normalized for the latitude variation of a small circle on a sphere. Channels are counted as many times as they cross parallels of latitude.

Figure 3 shows curves for S on a P-T_p diagram for values of the atmospheric emissivity, geostrophic wind, and heat transfer coefficient considered most likely. Other values of the atmospheric parameters result in climatic regimes of greater or lesser stability [see (*13*)]. However, all plausible solutions to our model show that the atmosphere can play an important role in the polar heat balance and that major climatic changes are likely. Because of the neglect of the greenhouse effect, P and T_p values at the upper right of Fig. 3 are somewhat below true values. Also shown in Fig. 3 is the vapor pressure curve of CO_2, which follows plausible S curves remarkably closely. A climate with stable polar caps occurs at the intersection of the dashed and solid curves appropriate to a particular value of S. We see that the present P corresponds to $S \simeq 1.9 \times 10^4$ erg cm^{-2} sec^{-1}, implying $T_p \simeq 145$°K, and $A = 0.76$ or 0.77. With scattering by aerosols in the polar hood, these values correspond well to present martian conditions. For $S \geqq 2.1 \times 10^4$ erg cm^{-2} sec^{-1} there is no stable intercept until $T_p \simeq 190$°K and $P \sim 1$ bar are reached. For S curves that are intersected three times by the vapor pressure curve, the middle intersection is unstable (*13*). Thus, for plausible values of the model parameters there exist two stable climatic regimes on Mars, one in the vicinity of the present conditions, and one at much higher pressures.

Not all conceivable models show double-valued curves (*13*). All of the models do, however, exhibit reversible climatic change. Single-valued solutions return to current conditions whenever S returns to present values. Double-valued solutions always return to present or lower-pressure environments for some decline in S. If the stable polar caps were not CO_2 but a CO_2-H_2O clathrate, the dashed curve in Fig. 3 would have a steeper slope, and the stability of the present environment would be enhanced.

If there is CO_2 equivalent to less than 1 bar in the polar caps, P at times of high S will be correspondingly less. The remnant polar caps have been found by Mariner 9 imagery (*14*) to be on layered terrain which is several kilometers thick, in agreement with an earlier crude estimate (*1*). If composed of some tens of percent volatiles [see (*14*)] and if completely vaporized they would produce $P \sim 1$ bar. On the implicit assumptions that deep patches of frozen volatiles are impossible, that low-albedo polar regions revealed by Mariner 9 are bare ground and not altered frost, and that buried volatiles are irrelevant for this problem, a much smaller equivalent pressure of CO_2, $P \simeq 40$ mbar, has been derived (*15*). We find these assumptions debatable. But even this low estimate is enough for running equatorial water on Mars.

Much larger quantities of CO_2 appear to have been outgassed during the history of Mars (*16*). If the ancient P were $\gtrsim 0.3$ bar, experience with models of the earth and Venus (*17*) implies that a CO_2-H_2O greenhouse would result which provides an increase of the order of 30°K in the global temperature. This is enough to have the diurnal mean equatorial temperature above the freezing point of water. (With large values of P, extensive stratospheric condensation of CO_2 seems possible, which may either cool the surface by increasing the global albedo or heat the surface by enhancing the greenhouse effect.) However, such temperatures are not required to cut the channels; terrestrial arctic rivers flow even when nighttime temperatures are well below 273°K.

The advective and greenhouse instabilities are separable, and only the

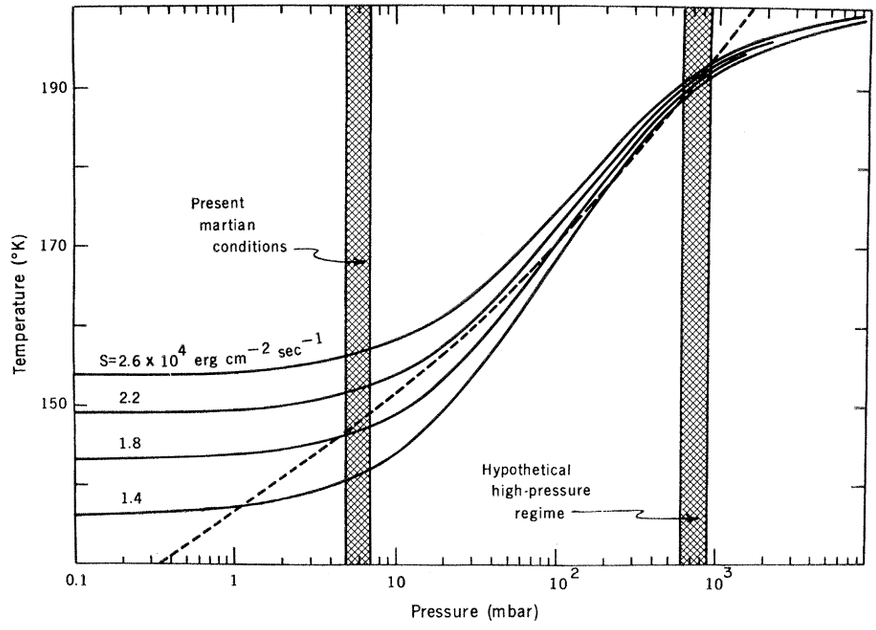

Fig. 3. Summary diagram for the outbreak of advective instability on Mars. (S) Solar flux absorbed in the polar cap; (dashed line) vapor pressure curve of CO_2. Stable climatic regimes occur only at the intersections of solid and dashed curves. For solid curves which are intersected three times by the dashed line, only the extreme intersections imply a stable climate. If $\leq$ 1 bar of CO_2 is buried in the martian polar regions, the high-pressure stable climate is determined by the total quantity of frozen CO_2. The calculations assume an atmospheric infrared emissivity of 0.1, an average wind speed of 5 m sec^{-1}, and a heat transport coefficient of 9×10^{-4}. These values are consistent with those assumed by Leovy and Mintz (*25*). Other values of these parameters are discussed in (*13*).

former is necessary to explain the channels. Runaway advection corresponds to a 15 to 25 percent increase in S. Such an increase can, in principle, be provided by a variation in any of the five variables in Eq. 1. We discuss in turn celestial mechanical variables, variable solar luminosity, and variable polar albedo.

A 15 percent increase in S corresponds to a decrease in a from 1.5 to 1.4 A.U., entirely inconsistent with the known stability of the martian orbit. Likewise, it corresponds to a variation of e from about 0.09 to about 0.49, while the maximum estimated value of e is about 0.13 (*18*). This leaves variations in δ, S_0, and A—which are also three fashionable variables in theories of climatic change on the earth (*19*). Obliquity driving of runaway advection requires an increase in δ from about 25° to about 31°. The computed maximum value of δ is about 35°, and the minimum value about 15°, with a period of $\sim 10^5$ years (*20*). Thus, it appears that the atmospheric pressure on Mars has been both much larger and much smaller than present values during a considerable portion of martian history. From obliquity driving alone, major excursions in pressure apparently occur in periods of the order of 10^5 years.

To explain the puzzlingly low solar neutrino flux, several models have emerged in which periodic mixing of ^3He in the sun produces a long-term variation both in the neutrino flux and in the solar luminosity. Current models (*21*) exhibit variations in S_0 typically ranging from about 7 to about 35 percent with the present epoch near the minimum value of S_0. Further evidence that luminosity fluctuations of G-type stars may be of this amplitude follows from an examination of the color magnitude diagram of the galactic star cluster Praesepe (*22*). Such solar flux driving would imply that ice ages on both the earth and Mars are relatively rare. The periods of such climatic variation would be greater than 10^8 years.

Finally, runaway advection can be driven by a decrease in the effective albedo of the polar cap from about 0.77 to about 0.73. Since the average bolometric albedo of martian dark areas is $\simeq$ 0.25, this corresponds to only a small admixture of dust. Albedo driving appears to be the most sensitive cause of advective instability. Epochs such as the present one in which great sand and dust storms exist and deposit particulates on the polar caps may be epochs in transition toward more clement conditions. High-pressure climates with abundant liquid water will remove dust from circulation, brighten the polar caps, and effect a transition toward low-pressure conditions. In our advective model, S must reach high values for periods of more than 80 years (*13*). Thus, annual dust storms cannot trigger climatic instability, although a period of centuries in which pervasive atmospheric particulates dirty the polar snows can. The incompletely solved problem of the generation of martian global dust storms is connected with larger problems of climatic instability on Mars. Despite the fact that the integrated sunlight is the same at both poles over a martian year, the period of equinoctial precession on Mars, which is roughly the period of variations in e (*18*), may be a characteristic period of the epochs of generation of global dust storms (*23*), and thus of varying A.

Accordingly, there may be three different periods of climatic variation on Mars, and some estimate of their relative values may emerge from high-resolution photography of the polar laminae by future space vehicles. This regularly terraced terrain is very likely produced by periodic climatic variations. While the foregoing instability mechanisms have been treated as independent, they are clearly interconnected. Although we have here employed only first-order models, it no longer appears miraculous to invoke reversible climatic instability to explain the channels and other features suggestive of extensive liquid water on Mars. Such an aqueous epoch on Mars has important biological and other geological implications (*1*). In particular, putative martian organisms which flourish in the aqueous epoch may now be in cryptobiotic repose, detectable by experiments utilizing liquid water in Mars landers such as on Viking. The model climatic instability described here may also be of some use in discussing the probably more difficult problem of climatic instability on the earth, and in considering—for example, by darkening the martian polar caps—possible intentional climatic modification of Mars (*24*).

CARL SAGAN
O. B. TOON, P. J. GIERASCH
Laboratory for Planetary Studies,
Cornell University,
Ithaca, New York 14850

References and Notes

1. C. Sagan, *Icarus* **15**, 511 (1971).
2. W. K. Hartmann, *J. Geophys. Res.*, in press; compare with C. Chapman, J. B. Pollack, C. Sagan, *Astron. J.* **74**, 1039 (1969).
3. C. Sagan, *J. Geophys. Res.*, in press; C. Sagan *et al.*, *ibid.*, in press.
4. W. M. Sinton, *Icarus* **6**, 222 (1967); R. Beer, R. H. Norton, J. V. Martonchik, *ibid.* **15**, 1 (1971).
5. J. Houck, J. B. Pollack, C. Sagan, D. Schaack, J. A. Decker, *ibid.* **18**, 470 (1973).
6. C. Sagan, J. Phaneuf, M. Ihnat, *ibid.* **4**, 43 (1965); see also A. Binder and D. P. Cruikshank, *ibid.* **5**, 522 (1966).
7. G. R. Hunt, L. M. Logan, J. W. Salisbury, *ibid.* **18**, 459 (1973).
8. B. Conrath *et al.*, *J. Geophys. Res.*, in press.
9. R. P. Sharp, L. A. Soderblom, B. C. Murray, J. A. Cutts, *ibid.* **76**, 331 (1971); D. Belcher, J. Veverka, C. Sagan, *Icarus* **15**, 241 (1971).
10. L. A. Soderblom, T. J. Kriedler, H. Masursky, *J. Geophys. Res.*, in press.
11. Liquid CO_2 as the excavating material requires implausibly large quantities of CO_2 to be today sequestered on Mars: CO_2 cannot escape from the planet. High-velocity streams of fluidized sand may exist on Mars, but the surface markers of high-speed winds do not correspond with the distribution of channels (*3*), and braided channels remain mysterious in this hypothesis.
12. R. B. Leighton and B. C. Murray, *Science* **153**, 136 (1966).
13. P. Gierasch and O. B. Toon, *J. Atmos. Sci.*, in press.
14. B. C. Murray, L. A. Soderblom, J. A. Cutts, R. P. Sharp, D. J. Milton, R. B. Leighton, *Icarus* **17**, 328 (1972).
15. B. C. Murray, M. C. Malin, S. C. Yeung, preprint.
16. The large martian volcanoes have volumes of the order of 10^{21} cm^3. Since the entire observable volume of such a volcano must be melted during its formation, and since we know (*5*) that $\sim$ 1 percent by mass of the martian surface material is water of crystallization (a typical value for terrestrial minerals as well), $\sim 10^{19}$ g of water vapor must have been released in the formation of each volcano. The concentration ratio $[CO_2]/[H_2O]$ for Mars is uncertain. Counting the oceans and the carbonates in the sedimentary column, it is $\sim$ 1/6 for the earth. In the atmosphere of Venus this ratio is $> 10^3$. Atmospheric abundances can be dominated by the vapor pressure curve of water. If we adopt $[CO_2]/[H_2O] \sim 1$ for the martian surface, then the evolution of a single large shield volcano releases over the whole surface of Mars $CO_2 \sim 10$ g cm^{-2} from the substance of the volcano itself. Allowing for gases vented from the martian interior; for the existence of several large shield volcanoes, many smaller ones, and the remnants of highly eroded ancient volcanoes (M. Carr, *J. Geophys. Res.*, in press); and for the great uplifted plateaus and ridges on which the volcanoes sit, a total outgassing over the history of Mars of $\gtrsim$ 1 bar of CO_2 does not appear implausible. Nitrogen has not been identified in the martian atmosphere, but this is not a good argument against extensive outgassing on Mars. In the absence of contemporary microbiological activity, most of the nitrogen in the earth's atmosphere would be present as nitrates in the crust.
17. C. Sagan, Technical Report TR 32-34, Jet Propulsion Laboratory, Pasadena, California (1960); A. P. Ingersoll, *J. Atmos. Sci.* **26**, 1191 (196 → S. I. Rasool and C. deBerg, *Nature* **226**, 1037 (1970); J. B. Pollack, *Icarus* **14**, 295 (1971); C. Sagan and G. Mullen, *Science* **177**, 52 (1972).
18. B. C. Murray, W. R. Ward, S. C. Yeung, *Science* **180**, 638 (1973).
19. See, for example, H. H. Lamb, *Climate: Present, Past, and Future* (Methuen, London, 1972).
20. W. R. Ward, *Science* **181**, 260 (1973).
21. D. Ezer and A. G. W. Cameron, *Nature Phys. Sci.* **240**, 180 (1972); F. W. W. Dilke and D. O. Gough, *Nature* **240**, 262 (1972); R. T. Rood, *Nature Phys. Sci.* **240**, 178 (1972); ———, W. A. Fowler, F. Hoyle, *Bull. Amer. Astron. Soc.*, in press.
22. C. Sagan and A. T. Young, *Nature* **243**, 459 (1973).
23. See, for example, G. S. Golitsyn, *Icarus* **18**, 113 (1973); G. Briggs, in preparation; P. Gierasch and R. M. Goody, *J. Atmos. Sci.*, in press.
24. C. Sagan, *The Cosmic Connection* (Doubleday, New York, in press); *Icarus*, in press; see also J. Burns and M. O. Harwit, *ibid.* **19**, 126 (1973).
25. C. Leovy and Y. Mintz, *J. Atmos. Sci.* **26**, 1167 (1969).

26. We are grateful to the members of the Mariner 9 scientific and engineering teams, and to our Mariner 9 colleagues with whom we have discussed the channels, particularly Bruce Murray, Harold Masursky, Daniel Milton, John McCauley, Paul Fox, and Joseph Veverka. We are indebted to Paul Fox for the compilation, to be published elsewhere, on which Fig. 2 is based. Supported in part by NASA grant NGR 33-010-082 and NASA/JPL contract 952487.

4 May 1973; revised 23 July 1973 ■

Montmorillonite: Electron-Optical Observations

Abstract. *Fine-grained micas are consistent impurities in Camp-Berteaux (Morocco) and Wyoming montmorillonites. These micas give selected-area electron diffraction spot patterns with triclinic, monoclinic, and hexagonal symmetries similar to those reported previously for montmorillonites. Camp-Berteaux montmorillonite appears as folded and flexible polycrystalline aggregates with pronounced texturing along the [02], [11], and [1$\bar{1}$] directions. Wyoming montmorillonite displays better crystallinity and larger crystallite size, and its structure is no longer truly "turbostratic."*

Montmorillonite is the principal mineral in bentonites, and therefore it is the most common smectite in nature. Because of its unusual physical properties, this mineral has a wide range of technical applications in fluids used in drilling oil wells, in the ferrous metal industry, in paper and pharmaceutical products, and so forth. These unusual properties of the mineral are related to its crystal structure, morphology, and particle size. A combination of a transmission electron image with a selected area electron diffraction (SAD) pattern provides probably the most effective means for studying the structure and morphology of this mineral. Extensive investigations along this line were carried out by Mering and Oberlin (*1*), who made excellent contributions to our understanding of this subject. They believed that they had obtained SAD patterns from single montmorillonite layers. Recently, SAD patterns were also published for single montmorillonite layers by Roberson and Towe (*2*). The investigators mentioned above, however, had no micrographs of the single montmorillonite layers giving rise to these diffraction patterns.

The symmetry determinations on montmorillonite single crystals by various investigators were not quite in agreement, although samples from the same type localities were studied. Specifically, Mering and Oberlin (*1*) proposed the space group $C2$ for the Wyoming montmorillonite, whereas others suggested triclinic (*2*) and hexagonal (*3*) symmetry for it. A similar situation exists for the Camp-Berteaux montmorillonite from Morocco.

I have carried out extensive electron-optical investigations on a large number of bentonites (*4*). Some of the results, which are summarized in this report, may provide an explanation for the discrepancy between the reports of other investigators. Observations on montmorillonites from two type localities, Camp-Berteaux and Wyoming, are discussed here.

The fractions of the samples less than 2 μm in equivalent spherical diameter were separated by centrifugation

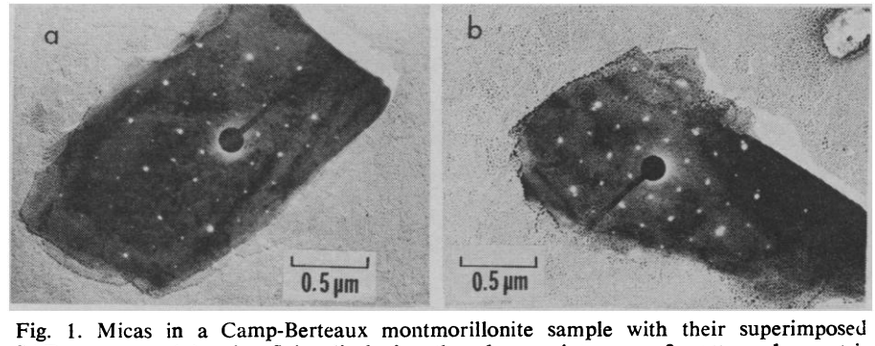

Fig. 1. Micas in a Camp-Berteaux montmorillonite sample with their superimposed SAD patterns: (a) mica flake displaying the plane point group 2 pattern, hence triclinic symmetry; (b) mica flake displaying hexagonal symmetry.